Predator-Prey Encounters Studied as Relative Particle Diffusion

J. Mann[1], S. Ott[2], H. L. Pécseli[3], and J. Trulsen[4]

[1] Risø National Laboratory, DK-4000 Roskilde, Denmark
jakob.mann@risoe.dk
[2] Risø National Laboratory, DK-4000 Roskilde, Denmark
soeren.ott@risoe.dk
[3] University of Oslo, Institute of Physics, Box 1048 Blindern, N-0316 Oslo, Norway
hans.pecseli@fys.uio.no
[4] University of Oslo, Institute of Theoretical Astrophysics, Box 1029 Blindern, N-0315 Oslo, Norway
jan.trulsen@astro.uio.no

Summary. The feasibility of an experimental method for investigations of the particle flux to an absorbing surface in turbulent flows is demonstrated in a Lagrangian as well as an Eulerian representation. A laboratory experiment is carried out, where an approximately homogeneous and isotropic turbulent flow is generated by two moving grids. The simultaneous trajectories of many small approximately neutrally buoyant polystyrene particles are followed in time. In a Lagrangian analysis, we select one of these as the centre of a "sphere of interception", and obtain estimates for the time variation of the statistical average of the inward particle flux through the surface of this moving sphere. The variation of the flux with the radius in the sphere of interception, as well as the variation with basic flow parameters is well described by a simple model, in particular for radii smaller than a characteristic length scale for the turbulence. Applications of the problem to, for instance, the question of the feeding rate of micro-organisms in turbulent marine environments are pointed out.

1 Introduction

Often the problem of turbulent diffusion in neutral turbulent flows is analysed in terms of an initial value problem [1, 2]. However, for many applications, a boundary value problem is more relevant. As such an example we here consider the turbulent particle flux to a perfectly absorbing spherical surface, which is a realistic physical model for many practical applications. This formulation of the problem serves, for instance, as a model for predator-prey encounters in turbulent waters, and seems to be the application of the problem that has received most attention recently [3, 4]. For small predators, fish larvae for instance [5], it can safely be assumed that their self-induced motion is small or negligible, and that they are passively convected by the local flow velocity, at least to a good approximation. Similarly, it can be assumed that their food (micro-zooplankton, for instance) is also passively convected by

the same flow. The feeding process can be modelled by assuming that any individual prey entering a suitably defined "sphere of interception" is captured with certainty. The surface is thus "virtual" in the sense that it does not disturb the flow.

In turbulent waters, the prey flux to a passively convected predator is related to the problem of relative diffusion, but now considered as a boundary value problem, with the sphere of interception acting as a perfect absorber of prey. This is the standard model for this particular problem [6,7]. We use this as a terminology in the following, for simplicity and definiteness. The general interest in the problem arises essentially from the simple observation that the food concentration in the near region of a predator will rapidly be depleted, and without any self-induced motion a predator will be starving, unless the prey within its sphere of interception is replaced by turbulent mixing in the surrounding flow. Although the results presented in this work explicitly refer to spherical volumes, the scaling laws that are obtained will have a wider range of applications.

We propose and demonstrate the feasibility of an experimental method for a quantitative study of turbulent transport into an absorbing surface, and present results for varying parameters [8]. It is demonstrated that a relatively simple model equation is adequate for describing the basic features of our observations. The paper is organized as follows; in Sect. 2 we give a short summary of the experimental set-up, and the experimental conditions. In Sect. 3 we discuss experimental results for particle fluxes to an absorbing sphere where the centre is identified by a particle which is moving with the flow. Section 4 contains a discussion of a simple analytical model which gives results in fair agreement with observations. Finally, Sect. 5 contains our conclusions.

2 Experimental Set-up

The basic features of the present experiment are described elsewhere [9, 10]. A short summary will suffice here. The turbulence is generated by the motion of two plastic grids, in the top and bottom of a tank with $320\times320\times450\,\mathrm{mm}^3$ inner dimensions, see Fig. 1 for a schematic illustration.

Typical Taylor micro-scale Reynolds numbers [11], $R_\lambda = \lambda^2/(\eta^2\sqrt{15})$, are ~ 100 for the present conditions, using the Taylor micro scale $\lambda = \sqrt{15\nu\sigma^2/\epsilon}$, where $\nu \simeq 0.89\,\mathrm{mm}^2/\mathrm{s}$ is the kinematic viscosity of the water, ϵ the specific energy dissipation rate, and σ^2 is the variance of one velocity component. The Kolmogorov length scale $\eta = (\nu^3/\epsilon)^{1/4}$ is less than $1/2\,\mathrm{mm}$ for the present conditions, while Kolmogorov time scales τ_η are in the range 0.05–0.12 s. The "micro-scale" η represents the length-scales, where the viscous effects become important. A characteristic Eulerian length scale, $\mathcal{L}_E$ as well as ϵ are determined by fitting a von Kármán type wavenumber spectrum [9,10] to the experimentally obtained data

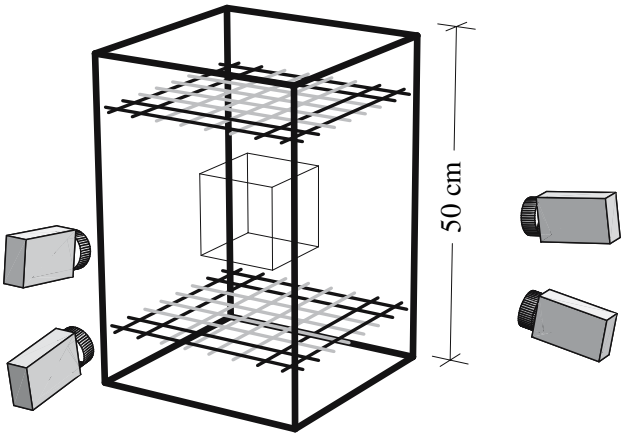

Fig. 1. Schematic illustration of the experimental set-up, showing the movable grids and the 4 video cameras. A restricted measuring volume of $140\times140\times120\,\mathrm{mm}^3$ is shown by thin lines

$$E(k) = \alpha\epsilon^{2/3}\mathcal{L}_E^{5/3}\frac{(\mathcal{L}_E k)^4}{[1+(\mathcal{L}_E k)^2]^{17/6}}\ , \tag{1}$$

where α is the spectral Kolmogorov constant [12]. $\mathcal{L}_E$ is found to be in the range 20–25 mm. We can interpret $\mathcal{L}_E$ as the lower limit for separations between fixed frame detection points, where the velocities of fluid elements tend to become uncorrelated. As a working hypothesis we can assume that velocities are also statistically independent for separations larger than $\mathcal{L}_E$. An integral length scale can be defined by the integral of the parallel velocity component correlation function $R_\parallel(r)$ as $\mathcal{L}_{\mathrm{int}} = \int_0^\infty R_\parallel(r)\mathrm{d}r$. A summary of parameters for 8 different conditions used in the present work is given in Table 1.

The motions of small polystyrene particles of size $a = 0.5 - 0.6$ mm are followed with 4 video cameras, and the simultaneous positions of typically 500–1000 particles recorded at time intervals of 1/25 s. The size of the effective measuring volume is approximately $140 \times 140 \times 120\,\mathrm{mm}^3$. It is ensured that the particles used in the experiment are approximately neutrally buoyant [9]. By a tracking procedure it is then possible to link the positions of particles [9], and thus to follow their individual motions in 3 spatial dimensions. In particular also their time varying velocity can be deduced. An illustrative sample trajectory is shown in Fig. 2. The figure shows a series of small spheres, centred at the particle positions, at individual sampling times. Since the time sequence used here is one of the longer ones obtained, the superposition of the spheres at subsequent sampling times gives rise to an appearance like a grey "band".

Experiments are carried out for different intensities of the turbulent velocity fluctuations, $\langle u^2\rangle$. With the polystyrene particles acting as markers for the

Table 1. Summary of the parameters derived from the second order structure function and the spectra obtained from it, based on measurements in the restricted volume shown in Fig. 1

$\alpha\epsilon^{2/3}$ ($\mathrm{mm}^{4/3}/\mathrm{s}^2$)	$\mathcal{L}_E$ (mm)	σ (mm/s)	$\mathcal{L}_{\mathrm{int}}$ (mm)	ϵ ($\mathrm{mm}^2/\mathrm{s}^3$)	τ_η (s)	η (mm)	λ (mm)	R_λ
45	31	18	23	160	0.075	0.26	5.1	100
41	27	16	20	140	0.080	0.27	4.9	88
40	29	16	22	135	0.081	0.27	5.1	93
45	28	17	21	160	0.075	0.26	4.9	91
24	29	12	22	62	0.120	0.33	5.8	81
65	29	21	22	279	0.056	0.22	4.5	104
56	28	19	21	225	0.063	0.24	4.6	97
25	27	12	20	65	0.117	0.32	5.6	78

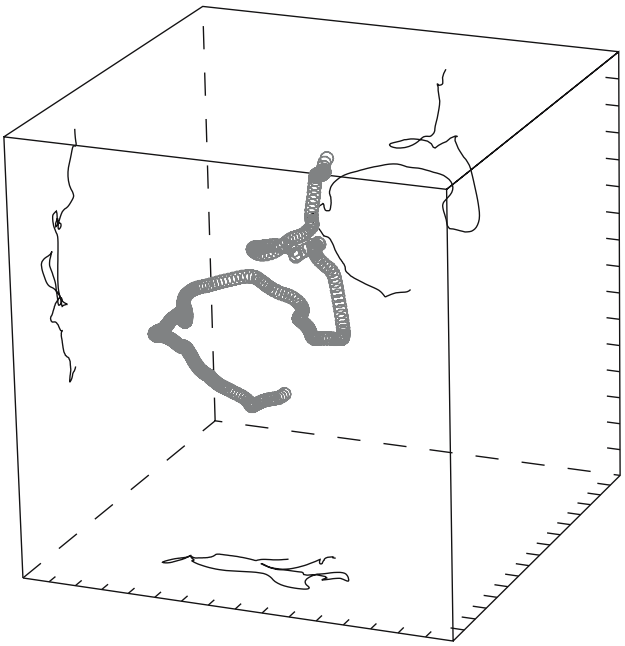

Fig. 2. Sample of particle trajectory obtained experimentally with 1/25 s time resolution. The small spheres give the particle position, and the continuous line a numerically interpolated particle trajectory, projected onto three of the bounding surfaces of the box. The distance between the tic-marks on axes is 10 mm. The spheres are here shown enlarged, for the sake of illustration

local flow velocities, experimental estimates can be obtained for the second order structure function, $\Psi_2(y) = \left\langle (u_i(\mathbf{r},t) - u_i(\mathbf{r}+\mathbf{y},t))^2 \right\rangle$ being independent of t for time stationary conditions. An example is shown in Fig. 3, including also a fit for small separations given by a dashed line, using the universal Kolmogorov $(\epsilon r)^{2/3}$ law. If we let the separation vector be along the y-axis, we have the longitudinal structure function $\Psi_{2\parallel}(y) \equiv \left\langle (u_y(0,t) - u_y(y,t))^2 \right\rangle$ given by the dotted line, with C_K being the Kolmogorov constant, related to the spectral constant α from (1) by $C_K \approx 1.315\,\alpha$ [12]. We note that C_K is known with some uncertainty, and a value of $C_K \approx 2.5$ can be justified as well as $C_K \approx 2.0$ [10,12]. The dash-dotted line in Fig. 3 gives the transverse structure function $\Psi_{2\perp}(y) \equiv \left\langle (u_x(0,t) - u_x(y,t))^2 \right\rangle$. By a general relation [11] we have

$$\Psi_{2\perp} = \frac{1}{2y} \frac{\mathrm{d}(y^2 \Psi_{2\parallel})}{\mathrm{d}y} \,,$$

for locally homogeneous and isotropic turbulence. With $\Psi_{2\parallel} \approx C_K(\epsilon y)^{2/3}$, we find $\Psi_{2\perp} \approx (4/3)\Psi_{2\parallel}$ in the universal subrange. The full line in Fig. 3 shows $\langle (\mathbf{u}(\mathbf{r},t) - \mathbf{u}(\mathbf{r}+\mathbf{y},t))^2 \rangle = 2(\langle u^2 \rangle - \langle \mathbf{u}(\mathbf{r},t) \cdot \mathbf{u}(\mathbf{r}+\mathbf{y},t) \rangle)$. The purpose of Fig. 3 is to demonstrate the existence of a universal range, and to indicate the range of its validity, here up to separations of the order of $20 - 25\,\mathrm{mm}$.

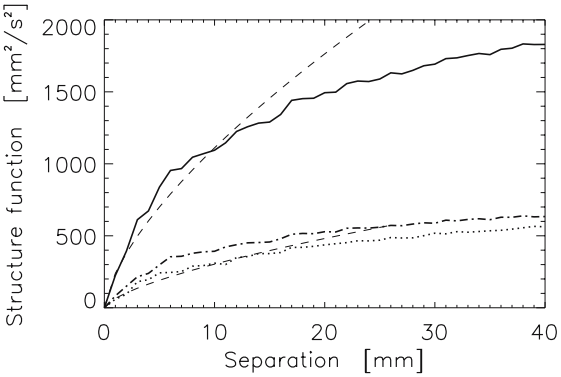

Fig. 3. Experimentally obtained second order structure function, as function of separation variable y. The heavy dashed line shows a $y^{2/3}$ fit. The *dotted line* refers to the longitudinal structure function, and the *dot-dashed line* to its transverse counterpart. The full line gives the structure function $\Psi_{2\parallel} + 2\Psi_{2\perp}$

The average distance between particles is much larger than their diameter, and particle interactions can be ignored. We estimate a Stokes number [13] as $St \equiv (2/9)(a/\mathcal{L}_E)^2 R_e$ with R_e being the Reynolds number based on $\sqrt{\langle u^2 \rangle}$ and $\mathcal{L}_E$. For typical values [10] of $\mathcal{L}_E = 25\,\mathrm{mm}$ and $R_e \approx 500$ we find $St \approx 0.05 \ll 1$. To the given accuracy, we assume that the particles follow the flow as passive tracers [14], and that the particle density is uniform, when

interpreting fluxes to an absorbing surface. The assumption was substantiated by analysing the particle distributions and comparing the results to a model Poisson distribution.

3 Particle Flux into a Moving Sphere

With the records for simultaneous particle trajectories being available, we can select one of them to represent the "predator" and label all the others as "prey". We then select a predetermined radius $\mathcal{R}$ in the sphere of interception, and then remove all the particles which happen to be inside this sphere at the initial time. During the subsequent Lagrangian motion of the reference "predator", we count the number of prey entering its co-moving sphere of interception between successive time steps. Each time a particle enters, it is "eaten" in the sense that it is removed from the database [8]. Of course, if the data analysis is carried out for very long times, all particles representing prey will eventually be removed. Here we are only interested in the time evolution of the prey flux for times up to an eddy turn-over time. As long as $\mathcal{R}$ is much smaller than the size of the measuring volume, we can with negligible error assume the prey concentration to be constant at large distances, corresponding to an ideally infinite system. By choosing a large number of realizations, we can give an estimate for the ensemble averaged Lagrangian prey flux as a function of time after release.

In Fig. 4 we show, with solid lines, examples of the time varying particle flux to a self consistently moving sphere of interception with a given radius, $\mathcal{R}$. This flux is the result of a competition between, on one hand, the depletion of the density of polystyrene particles in the near vicinity of the reference sphere

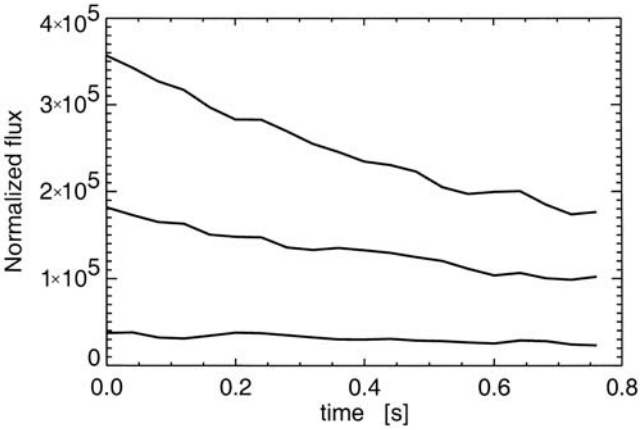

Fig. 4. Time variation of the estimate for the averaged particle flux for unit density $\langle J(t)\rangle/n_0$, to moving spheres, with radii, $\mathcal{R} = 10$, 20 and 30 mm

as they "absorbed", and, on the other hand, inward flux of such particles, due to the turbulent motions in the flow. In each realization, we divide the flux by the particle density for that particular realization. The result thus represents the particle flux for unit particle density, i.e. 1 particle per mm^3. For small radii, $\mathcal{R} < \mathcal{L}_E$, we find that the flux level is almost constant in time. A decreasing trend becomes more conspicuous as the radius is increased, and for $\mathcal{R} > \mathcal{L}_E$ we find a significant flux reduction for times approaching the eddy turn-over time, here estimated by $\tau_F \equiv \mathcal{L}_E/\sigma$. The flux is largest initially, when the concentration of "prey" in the surrounding is largest. At later times there will be a possibility for encountering fluid elements which *have* already been emptied, and the prey flux becomes smaller. The flux depletion due to this effect increases evidently for increasing radii in the reference sphere.

4 Analytical Results

The problem of turbulent particle flux to a perfect absorber moving with the flow can be studied analytically by allowing for some simplifying assumptions. Here, an absorbing spherical surface is assumed to have its centre defined by a particle, which is moving with the flow.

4.1 Dimensional Arguments

The present problem is characterized by a few dimensional quantities. With the viscosity, ν, being immaterial for the flow dynamics for scale lengths larger than the Kolmogorov length scale $\eta \equiv (\nu^3/\epsilon)^{1/4}$, we only have one quantity characterizing the turbulent flow, namely ϵ with dimension $\mathit{length}^2/\mathit{time}^3$, and the length scale $\mathcal{R}$ characteristic for the particular problem, here a moving sphere of interception. Out of these quantities the only combination giving a quantity with dimension *time* is $\mathcal{R}^{2/3}/\epsilon^{1/3}$, while $\epsilon^{1/3}\mathcal{R}^{7/3}$ gives $\mathit{length}^3/\mathit{time}$. The physical dimension of the averaged normalized particle flux $\langle J \rangle / n_0$ is $\mathit{length}^3/\mathit{time}$.

Quite generally it can then be argued, by purely dimensional reasoning, that the turbulent flux for given reference density n_0 must have the form

$$\frac{\langle J \rangle}{n_0} = \epsilon^{1/3}\mathcal{R}^{7/3} f\left(t\epsilon^{1/3}/\mathcal{R}^{2/3}\right) , \tag{2}$$

with f being a dimensionless function of a dimensionless variable. The actual form of f can only be determined by a more detailed model analysis. We can argue that we, in Fig. 4, have determined f experimentally, without reference to any explicit model equations. The arguments do not depend on any specific shape of the reference volume, and assume only that it scales self-similarly with one length scale, $\mathcal{R}$. The functional dependence f in (2) will, of course, be different for different shapes of the volume. Note that for $t > \mathcal{R}^{2/3}/\epsilon^{1/3}$,

see Fig. 4, the variation of $f(\tau)$ is rather slow for parameters relevant here. The observations summarized in Fig. 4 seem to indicate that f approaches a constant value for large times. The constant is assumed to be universal, and we find it here to be in the range 5–10, as discussed in more detail later. The observation is not as trivial as it might seem [15].

4.2 A Model Diffusion Equation

The particle flux to a perfectly absorbing sphere, which is moving with the flow has been modelled by, for instance, a simple diffusion equation with a properly chosen diffusion coefficient which depends on the simultaneous mean square velocity differences obtained at given spatial separations, but independent of time [7]. Essentially, the argument is based on the second order structure function

$$\Psi_2(r) \equiv \left\langle \left(u_r(0,t) - u_r(r,t)\right)^2 \right\rangle \approx C_K(\epsilon r)^{2/3} \,, \tag{3}$$

with the approximation being valid for separations r smaller than the length scale of the turbulence, see Fig. 3. A diffusion coefficient is constructed from a characteristic velocity and a characteristic length. The velocity is taken to be $\sqrt{\Psi_2(r)}$. For the limiting form expressed in (3), the only length characterizing the two particles is their separation r. The resulting diffusion coefficient is consequently $K(r) \sim r^{4/3}\epsilon^{1/3}$. The proposed diffusion equation for the density n is actually identical to the one suggested by Richardson in his study of distance-neighbour functions [16]

$$\frac{\partial}{\partial t} n(r,t) = C\frac{\epsilon^{1/3}}{r^2}\frac{\partial}{\partial r} r^{10/3}\frac{\partial}{\partial r} n(r,t) \,. \tag{4}$$

The result is written for spherically symmetrical geometry, with r being the radial coordinate, measured from the position of the centre of the reference sphere, and C is a numerical constant, assumed to be universal. While (4) was here argued by dimensional reasoning, it has also an analytical derivation [2]. As a consequence of (4) we have the well-known result for the mean-square separation of two initially close particles $\langle r^2 \rangle = C_R \epsilon t^3$, with the Richardson constant being $C_R \approx 0.5$ [10]. We have the relation $C = (3/2)(3C_R/143)^{1/3}$, giving $C \approx 0.33$. In the present model, the time varying diffusion flux of particles to a perfectly absorbing sphere is given by

$$J(t) = 4\pi C \epsilon^{1/3} \mathcal{R}^{10/3} \left.\frac{\mathrm{d}n(r,t)}{\mathrm{d}r}\right|_{r=\mathcal{R}} \,,$$

with $n(r,t)$ obtained from (4).

The derivation of (4) assumes that ϵ is a deterministic constant, and thereby ignores intermittency corrections [17]. Although the relation (4) had some experimental support from the time when it was first proposed [16],

and also supported more recently [10], its general validity has been criticized [1, 2], as also summarized recently [10]. The range of validity of (4) is thus not fully explored. For large separations, a simple diffusion equation, with constant diffusion coefficient, is expected to apply, as indicated for instance by experimental results [18], for initial conditions having scales larger than the integral length scale. These cases [10, 18] referred to particle releases considered as initial value problems. It seems that a diffusion equation as (4) can indeed be applied for analysing relative two-particle diffusion in certain variable ranges [10]. On the other hand, one cannot expect a diffusion coefficient depending solely on relative times or spatial separations to be universally applicable for this problem [2]. In general, a Fokker–Planck equation, with (4) being one special example, describes a Markov process, where the probabilities of future states depend solely on the present, and not past ones. Modelling of turbulence as a simple Markov process is known to be rather inaccurate, and a study of the limits of applicability of models like (4) is therefore worthwhile.

From (4) is easy to derive [7] a steady state flux to a sphere with radius $\mathcal{R}$ as

$$\frac{J_0}{n_0} = \frac{28\pi}{3} C \epsilon^{1/3} \mathcal{R}^{7/3} \ . \tag{5}$$

where n_0 is the constant particle density at $r \to \infty$.

4.3 Comparison Between Analytical and Experimental Results

In order to compare our observations with analytical results, we show by open circles in Fig. 5, the flux value at a time $t = \tau_F/2$, with τ_F being the eddy turn-over time. This time is sufficiently short to give a large number of

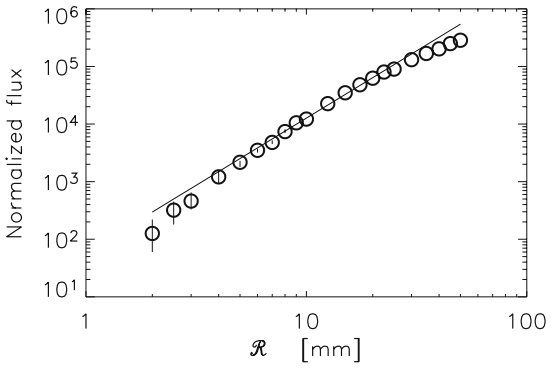

Fig. 5. The particle flux, $\langle J \rangle / n_0$, to a moving sphere of interception is shown with open circles for different radii, as is measured at 1/2 eddy turn over time, $t = \tau_F/2$. The full line gives the time-asymptotic result (5). Parameters are $\sigma = 19\,\mathrm{mm/s}$, $\tau_F = 1.6\,\mathrm{s}$, and $\epsilon = 225\,\mathrm{mm}^2/\mathrm{s}^3$. The fluxes are normalized to unit density

particle traces for the averaging, and on the other hand, sufficiently long to give an estimate close to the asymptotic flux value of the particle flux. Vertical lines give the uncertainties on the experimental estimates. For small radii $\mathcal{R}$, this uncertainty is large because we only seldom find close particles. For $\mathcal{R} > 5\,\mathrm{mm}$, on the other hand, this uncertainty is smaller than the size of the circles in Fig. 5. The analytical curve, given by a full line, is the asymptotic limit from (4), where we used $\epsilon = 225\,\mathrm{mm}^2/\mathrm{s}^3$. Taking into account that we have not introduced any free or adjustable parameters, we find the agreement between the analytical and experimental results to be satisfactory, although we note a slight, but systematic, reduction of the measured flux as compared with the analytical asymptotic result. The experimental results for the smallest radii give an underestimate, since in this limit a nontrivial fraction of the particles are "glancing", i.e. they manage to pass through the reference sphere within one sampling time, and are therefore not counted.

The model equations become inadequate for spatial separations larger than the largest eddies in the turbulence, $r \geq \mathcal{L}_E$, although we find that the $\mathcal{R}^{7/3}$-scaling seems to have a wider range of validity, in particular at early times, $t < \tau_F/2$. The analysis summarized here refers explicitly to spherical volumes. Qualitatively, the arguments will apply to different shapes as well, as long as they scale self-similarly with *one* characteristic length, $\mathcal{R}$.

We also present results for the flux variation for a fixed value of the radius of the moving sphere of interception, $\mathcal{R} = 20\,\mathrm{mm}$, and varying ϵ, see Fig. 6. In order to sample each dataset at a consistent time, we present results for a selected time $\tau_F/2$ used also in Fig. 5, using the proper value of σ. In this limit, we can in all cases assume that the particle flux is close to its asymptotic, or saturated, level. The circles show the result for ϵ obtained by fitting the second order structure function. Other methods for determining ϵ can be found, however [9], and these results are used to give the horizon-

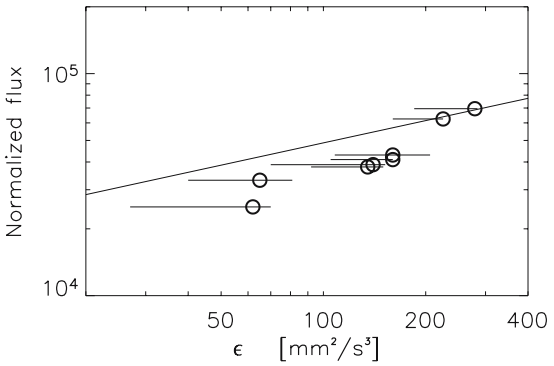

Fig. 6. Variation of the normalized flux, $\langle J \rangle / n_0$, with varying ϵ for a fixed value of $\mathcal{R} = 20\,\mathrm{mm}$. The full line gives the time-asymptotic result obtained from (4). See also Fig. 5

tal uncertainty bars. The theoretical full line is also in this case obtained as the asymptotic limit of the solution of Richardson's diffusion equation, using the most recent experimental value [10] of Richardson's constant. Within the range of variability, we find the scaling with ϵ to agree reasonably well with theoretical predictions based on (4). The numerical agreement between the measurements and analytical results is within a factor of 2, the analysis predicting a slightly larger flux than the observed value, also in agreement with the results shown in Fig. 5. The selected value $\mathcal{R} = 20\,\mathrm{mm}$ can be taken as representative for the length scales smaller than or equal to $\mathcal{L}_E$ in the experiments.

The results summarized in Figs. 5 and 6 refer to fluxes obtained at fixed normalized times. We can also demonstrate a scaling law for the time variations of these fluxes, and compare the results to the results from a model like the one given by (4). In Fig. 7 we show the normalized fluxes for 8 different experimental conditions, see Table 1, and radii $\mathcal{R} = 5$, 6, 7, 8, 9, 10, 12.5, 15, 17.5 and 20 mm. The figure demonstrates the experimental scatter, which is consistent with the uncertainties of the estimates for ϵ. Also here we note a "banded" structure in the figure. We find that the uppermost group of curves originates from the two datasets with the largest ϵ-values, see for instance also Fig. 6, where these two datasets also seem to be slightly distinct from the others.

Again, we note that the results have a wider range of applicability, and need not refer explicitly to spherical forms. A change in shape of the reference volume, will only imply a change in the numerical constant. Thus, the scaling law implied in Fig. 6 will apply, for instance, to the prey flux for any predator, independent of its range of vision, when it is exposed to different turbulence intensities.

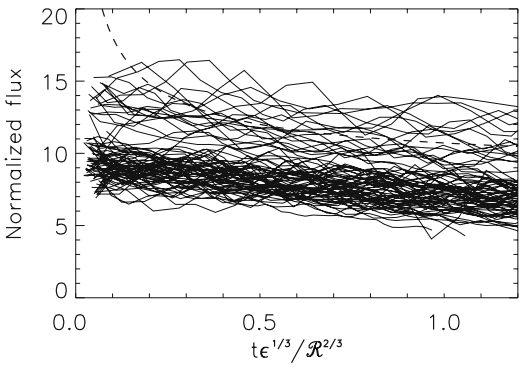

Fig. 7. Normalized flux, $\langle J \rangle / (n_0 \epsilon^{1/3} \mathcal{R}^{7/3})$, as a function of the normalized temporal variable, $t\epsilon^{1/3}/\mathcal{R}^{2/3}$. Curves are shown for 8 realizations with different turbulence conditions, each with curves for different $\mathcal{R}$. The dashed line gives a theoretical result, obtained from (4). The (unphysical) singularity at $t = 0$ for the full line solution is due to the assumed infinite initial gradient at $r = \mathcal{R}$

Given the experimental uncertainties, the scaling relations obtained by dimensional reasoning are found to be well satisfied when analysing the data from the present experiment. The more specific diffusion equation model (4), is only giving qualitative agreement for the measured Lagrangian fluxes at early times. It seems, however, that the asymptotic limit is well accounted for by the model, in particular also the numerical coefficient obtained by use of the most recent value of the Richardson constant [10]. To some extent, the modest agreement between the model and the experimental results at early times might be surprising, since (4) has given better agreement with estimates of the distance-neighbour functions [10]. We note, however, that in the present case there is an ambiguity in the model for the diffusion coefficient: the result (4) uses characteristic eddies being of magnitude comparable to the predator-prey separation [7], which is the most obvious choice when modelling an equation for the distance-neighbour function. For the present case, it could as well be argued that the characteristic eddies should have a size comparable to the separation distance between prey and the surface of interception. Since such models can serve as guidelines only, we shall not pursue the problem any further here.

As particles are absorbed by the surface, with fluxes shown in Fig. 7, the particle density will be depleted in the flow surrounding the moving reference sphere. We can analyse also here the average particle density for $r > \mathcal{R}$, as a function of time, with results shown in Fig. 8. The radius $\mathcal{R}$ is chosen to be in the universal subrange. The first curve is shown at the first sampling time, i.e. $t = 1/25\,\mathrm{s}$. Variations with distance are obtained in "bins" of 1 mm, and the second bin from the surface at $r = \mathcal{R}$ is the first one shown. To reduce the noise level, we normalized also here the curves with the radial density variation found at $t = 0$. If we choose a smaller value for $\mathcal{R}$, the noise level increases, while larger $\mathcal{R}$ will fall outside the universal subrange.

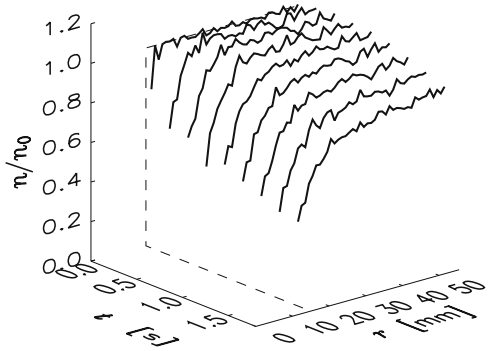

Fig. 8. Time evolution of the normalized density around an absorbing spherical surface moving with the flow, for $\mathcal{R} = 15\,\mathrm{mm}$

5 Conclusions

In this correspondence we investigated the turbulent flux to a perfectly absorbing surface, with particular attention to the problem of predator-prey encounters in turbulent flows. We summarized the basic elements of an experimental method for investigating the prey flux to a moving predator. In the limit of small $\mathcal{R}$, we found evidence for an $\mathcal{R}^{7/3}$ flux scaling (see Fig. 5) in terms of the radius of the sphere of interception. We also found indications of an $\epsilon^{1/3}$ scaling with the turbulent dissipation rate (see Fig. 6), in agreement with the predictions of the model (4). This model agrees to some extent also quantitatively with the observations. In the asymptotic time limit, to the extent it can be reached in the present experiment, the data gives a flux well approximated by (5), provided $\mathcal{R} < \mathcal{L}_E$. This will in general be the limit relevant for marine environments [19]. We suppose that the observations justify extrapolation to radii, $\mathcal{R}$, smaller than those experimentally accessible. In a general sense, our results provide experimental evidence also for the importance of turbulent motion for the feeding process in marine environments. We expect that in order to obtain a general analytical model, which can give results for extended time periods and all $\mathcal{R}$, we shall have to allow for a diffusion coefficient which depends on time as well as spatial separations, in particular including also memory effects [2].

The turbulent flux to a moving sphere can be significantly smaller than the flux to a stationary one. This can be argued simply by noting that the relative mean square velocity of a particle convected past a stationary sphere is $\langle u^2 \rangle$, while it is $\langle (\mathbf{u}(\mathbf{r},t) - \mathbf{u}(\mathbf{r}+\mathbf{y},t))^2 \rangle$, for a passively convected sphere-particle pair, with separation $\mathbf{y}$. For small separations, $y \ll \mathcal{L}_E$, we have [7, 20] the result (3), and the relative velocity is small, implying a small flux to the passively convected sphere. For large separations, $y \gg \mathcal{L}_E$, on the other hand, $\mathbf{u}(\mathbf{r},t)$ and $\mathbf{u}(\mathbf{r}+\mathbf{y},t)$ can be supposed to be statistically independent. The mean square relative velocity is then $2\langle u^2 \rangle$. The flux in this latter case is expected to be larger than that to the stationary sphere with a factor $\sqrt{2}$, although such large separations cannot be achieved for the present experimental conditions.

We can define a "gain factor" as the ratio between the flux to a stationary sphere divided by the flux to the passively convected sphere with the same radius, $\mathcal{R}$. In Fig. 9 we show this gain factor for various radii, $\mathcal{R}$. All points are obtained at the reference time $\tau_F/2$ used before. We find that the gain factor is considerable for small spheres of interception, using the length scale $\mathcal{L}_E$ as a measure. For $\mathcal{R} \approx \mathcal{L}_E$ this gain factor is close to 1, and the particle flux is the same for a stationary as for the moving sphere. For larger values, $\mathcal{R} > \mathcal{L}_E$, the flux to a moving sphere exceeds that to a stationary one. The variation of the initial value of the fluxes seen, for instance, on Fig. 4 are consistent with these observations. Heuristically, we can argue for a parameter variation of the gain factor as given by the ratio of the two scaling laws obtained by dimensional arguments, which here gives $\sigma/(\epsilon\mathcal{R})^{1/3}$. This ratio is shown by

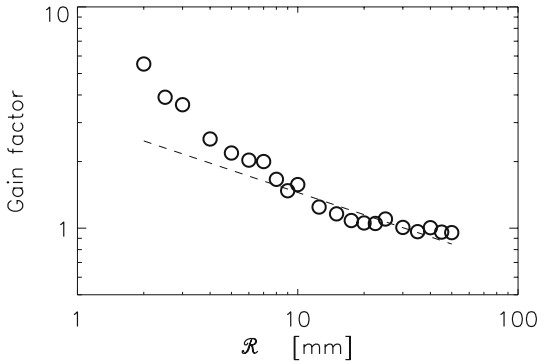

Fig. 9. Variation of the gain factor for a stationary sphere for various radii of the sphere of interception, $\mathcal{R}$. The figure refers to a time $t = \tau_F/2$.

a dashed line in Fig. 9, with a numerical constant not accounted for. We find, in this case, that this scaling law does not follow the data points in any convincing way, although the *trend* seems reasonable. After all, neither the Eulerian nor the Lagrangian data followed the scaling perfectly, the Eulerian data best at small $\mathcal{R}$, the Lagrangian data best at somewhat intermediate values. To expect a perfect agreement for the *ratio* of the two quantities may seem somewhat optimistic, in particular also because a small mean flow in the system gives a bias for the Eulerian fluxes. The gain factor shown in Fig. 9 can, for instance, be interpreted as the gain in prey flux for an imagined predator with possibilities for self-induced motion, which it uses to exactly compensate the motions in the surrounding water.

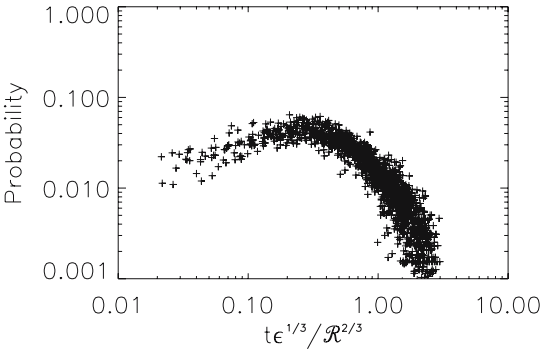

Fig. 10. Lagrangian transit time distribution, shown as a function of normalized temporal variable $t\epsilon^{1/3}/\mathcal{R}^{2/3}$. The figure contains 6 experimental conditions with ϵ = 62, 65, 135, 160, 225, and 279 $\mathrm{mm}^2/\mathrm{s}^3$, and each of these analysed for radii $\mathcal{R}$ = 5, 10, 15, and 20 mm

The present analysis, when applied to the predator-prey problem implicitly assumes that prey is captured with certainty. This might be an acceptable assumption for slow motions in the flow, but evidently it might become questionable when the flow is strongly turbulent. Little seems to be known about the capture probability of prey, when the relative velocities are large, although *some* observations have been quantified [21]. These results refer seemingly only to relatively large predators, fish larvae for instance. We can not here add to that discussion, but might note that one possibly essential part of the information, relevant for a detailed discussion, might be the distribution of transit times for prey through the sphere of interception. Also this question can be analysed on the basis of the present experimental data [15]. We can thus obtain the distribution of transit times taken as the time difference from a particle entering a reference sphere until it leaves it again for the first time (i.e. first passage time distributions). It turns out that also this distribution follows a seemingly universal scaling, as long as the radius of the moving reference sphere is within the universal subrange.

The problem discussed in the present communication is evidently of general interest. It has implications also for coagulation processes in turbulent colloids, for instance. A detailed investigation of this latter problem can, however, not be made by experiments like ours because the volume of the particles change upon coagulation, with a consequent change in their response to the turbulent flow motions. We can not reproduce this effect, for evident reasons. In standard studies of this problem [22], restricted to diffusion by Brownian motion, this effect is in part also ignored. With the same assumption it is possible to perform the relevant studies in experiments like ours, with results having implications for the formation rate of coagulants larger than the Kolmogorov scale η in turbulent flows.

Acknowledgement

Valuable discussions with Maria Pécseli in the initial stages of the project are gratefully acknowledged. This work was in part supported by the Danish Technical Research Council under contracts STVF-9601244 and 26-01-0087. Two of the authors (HLP and JT) were in part supported by the "Effects of North Atlantic Climate Variability on the Barents Sea Ecosystem" (ECOBE) project. The present study was completed while two of the authors (HLP and JT) were affiliated with the Norwegian Center for Advanced Studies.

References

1. G. K. Batchelor: Proc. Cambridge Philos. Soc. **48**, 345 (1952)
2. P. H. Roberts: J. Fluid Mech. **11**, 257 (1961)
3. S. Sundby, P. Fossum: J. Plankton Res. **12**, 1153 (1990)

4. T. Kiørboe, E. Saiz: Mar. Ecol. Prog. Ser. **122**, 135 (1995)
5. J. H. Muelbert, M. R. Lewis, D. E. Kelley: J. Plankton Res. **16**, 927 (1994)
6. B. J. Rothschild, T. R. Osborn: J. Plankton Res. **10**, 465 (1988)
7. T. Osborn: J. Plankton Res. **18**, 185 (1996)
8. J. Mann, S. Ott, H. L. Pécseli, J. Trulsen: Phys. Rev. E **65**, 026304 (2002)
9. J. Mann, S. Ott, J. S. Andersen: Technical Report No. Risø-R-1036(EN), Risø National Laboratory, DK-4000 Roskilde, Denmark (unpublished), can be downloaded from http://www.risoe.dk/rispubl/VEA/ris-r-1036.htm
10. S. Ott, J. Mann: J. Fluid Mech. **422**, 207 (2000)
11. J. O. Hinze: *Turbulence*, 2nd edn (McGraw-Hill, New York 1975)
12. A. S. Monin, A. M. Yaglom: *Statistical Fluid Mechanics* (The MIT press, Cambridge, Massachusetts, 1975), vol. 2
13. A. Babiano, J. H. E. Cartwright, O. Piro, A. Provenzale: Phys. Rev. Lett. **84**, 5764 (2000)
14. M. R. Maxey, J. J. Riley: Phys. Fluids **26**, 883 (1983)
15. J. Mann, S. Ott, H. L. Pécseli, J. Trulsen: Phys. Rev. E **67**, 056307 (2003)
16. L. F. Richardson: Proc. Roy. Soc. London, Ser. A **6**, 709 (1926)
17. G. Boffetta, A. Celani, A. Crisanti, A. Vulpiani: Phys. Rev. E **60**, 6734 (1999)
18. M. Virant, T. Dracos: Meas. Sci. Technol. **8**, 1529 (1997)
19. P. S. Hill, A. R. M. Nowell, P. A. Jumars: J. Mar. Res. **50**, 643 (1992)
20. S. Chandrasekhar: J. Madras Univ. B **27**, 251 (1957)
21. B. R. Mackenzie, T. Kiørboe, Limnol. Oceanogr. **45**, 1 (2000)
22. S. Chandrasekhar. In: *Selected Papers on Noise and Stochastic Processes*, ed by N. Wax (Dover, New York 1954), pp 3–91